

## Forcing singular vectors and other sensitive model structures

By J. BARKMEIJER<sup>1\*</sup>, T. IVERSEN<sup>2</sup> and T. N. PALMER<sup>1</sup>

<sup>1</sup>*European Centre for Medium-Range Weather Forecasts, UK*

<sup>2</sup>*University of Oslo, Norway*

(Received 30 May 2002; revised 28 January 2003)

### SUMMARY

Model tendency perturbations can, like analysis perturbations, be an effective way to influence forecasts. In this paper, optimal model tendency perturbations, or forcing singular vectors, are computed with diabatic linear and adjoint T42L40 versions of the European Centre for Medium-Range Weather Forecasts' forecast model. During the forecast time, the spatial pattern of the tendency perturbation does not vary and the response at optimization time (48 hours) is measured in terms of total energy. Their properties are compared with those of initial singular vectors, and differences, such as larger horizontal scale and location, are discussed. Sensitivity calculations are also performed, whereby a cost function measuring the 2-day forecast error is minimized by only allowing tendency perturbations. For a given number of minimization steps, this approach yields larger cost-function reductions than the sensitivity calculation using only analysis perturbations. Nonlinear forecasts using only one type of perturbation confirm an improved performance in the case of tendency perturbations. For a summer experiment a substantial reduction of the systematic error is shown in the case of forcing sensitivity.

KEYWORDS: Model error Optimal forcing

### 1. INTRODUCTION

The search for sensitive structures in weather forecasting is usually associated with the implications of sensitive dependence on initial conditions, commonly called 'the butterfly effect' (Gleick 1987). Many numerical weather-prediction (NWP) centres have now developed approaches to find fast-growing perturbations of the initial state and to use this knowledge in their ensemble forecasting. However, although such a technique is an essential tool to gain insight into possible weather scenarios, it is more and more recognized that solely perturbing the initial condition is not entirely adequate and that uncertainties in the mathematical description of subgrid-scale processes should also be treated in a probabilistic manner (see Houtekamer *et al.* (1996), Buizza *et al.* (1999) and Mylne *et al.* (2002)).

Modern NWP models are based on the equations of motion, truncated at a certain spatial scale, combined with an intricate balance of physical parametrizations, which describe complex processes, such as the formation of clouds. During the last few decades, substantial progress has been made in improving the quality of forecasts (see, for example, Simmons and Hollingsworth (2002)). Nevertheless, uncertainty in parametrization schemes will always limit forecast accuracy.

Tendency errors can be considered as a measure of instantaneous model error. They are defined as  $\mathbf{R}$  in the following equation

$$d\mathbf{x}_o/dt = d\mathbf{x}_m/dt + \mathbf{R}, \quad (1)$$

where  $\mathbf{x}_m$  denotes a prognostic model variable and  $\mathbf{x}_o$  denotes the same variable as resulting from observations. Klinker and Sardeshmukh (1992) studied one-step model integrations to obtain estimations of tendency errors. By switching off various parametrizations, they were able to isolate the contribution of different terms to the tendency error. On longer time-scales, a basic requirement of an NWP model is to possess realistic long-term flow statistics. A typical example of systematic error, i.e. the

\* Corresponding author, present address: Royal Netherlands Meteorological Institute, PO Box 201, 3730 AE De Bilt, the Netherlands. e-mail: barkmeij@knmi.nl

© Royal Meteorological Society, 2003.

difference between the model climate and the observed climate, is an excessively zonal mid-tropospheric circulation; this can become a dominant source of forecast inaccuracy for the seasonal time-scale (Branković and Palmer 2000). It is not straightforward to determine which physical parametrizations in the model require adjustment in order to improve the model climate. A procedure which is sometimes used for simple models to reduce systematic errors is to compute a time-independent forcing of model tendencies based on observed fields. By writing the model in the form

$$dx/dt = G(\mathbf{x}) + \mathbf{f}, \quad (2)$$

where  $G$  is the total model tendency, the additional forcing  $\mathbf{f}$  is computed by inserting observed fields for  $\mathbf{x}$ . Following Roads's (1987) 'residual tendency' procedure, the forcing  $\mathbf{f}$  can actually be computed by requiring that, for a long series of observed fields, the mean tendencies become negligible. With this technique it is possible to obtain a satisfactory model climate even for relatively simple models. See, for example, Marshall and Molteni (1993) who successfully applied it in the context of a three-level quasi-geostrophic model.

The forcing term  $\mathbf{f}$  as defined by Roads's procedure can be interpreted as a crude way to account for processes that are not explicitly or not entirely correctly described by the model equations. There are of course various ways to represent model error and several other approaches have been developed which have sometimes become part of operational weather-prediction models (for an overview see Palmer (2001)). An example of representing the uncertainty in model parametrization schemes is formulated by Buizza *et al.* (1999). Their approach ('stochastic physics') is to add stochastic noise in regions where the subgrid parametrization schemes are active. By splitting  $G$  into two terms,  $D$  and  $P$ , associated with tendencies of the adiabatic model component and physical parametrizations respectively, they propose a model forcing  $\mathbf{f}$  of the form:

$$\mathbf{f}(t) = \lambda P(\mathbf{x}), \quad (3)$$

where  $\lambda$  is a stochastic variable drawn from a uniform distribution in  $[-0.5, 0.5]$ . The scheme is used in the Ensemble Prediction System (EPS) at the European Centre for Medium-Range Weather Forecasts (ECMWF) with random drawings constant over a time range of 4.5 h and in a spatial domain of  $10^\circ \times 10^\circ$  latitude/longitude with each ensemble member using a different realization of  $\lambda$  (Buizza *et al.* 1999). In a study of the performance of the ECMWF EPS with special focus on tropical cyclones (Puri *et al.* 2001), the impact of stochastic physics was quite noticeable. The ensemble showed sensitivity to the different realizations of stochastic physics used in each ensemble member and, in particular, with respect to the intensity of tropical cyclones.

In this paper, we are interested in model forcings  $\mathbf{f}$ , which are constant in time but, when used as tendency perturbations, result in large perturbation growth in some measure during a given forecast period. In view of this, such  $\mathbf{f}$  structures will be referred to as *forcing singular vectors*. D'Andrea and Vautard (2000) study similar structures as a way to reduce systematic error in a quasi-geostrophic model. So-called *stochastic optimals* used by Moore and Kleeman (1999) in a coupled ocean-atmosphere model of the El Niño Southern Oscillation (ENSO) bear resemblance to forcing singular vectors but allow for time-dependent forcings  $\mathbf{f}(t)$ . By introducing stochastic optimals in the ENSO model, they obtained variability on seasonal-to-interannual time-scales with spectral characteristics similar to those seen in nature. However, their approach is not feasible in a realistic high-dimensional NWP model even for time-independent stochastic optimals because of their explicit computation in matrix form of the propagator of the linear model and its adjoint.

In section 2, the concept of forcing is illustrated with two examples which are usually associated with defining sensitive patterns in the initial condition: the singular vector and sensitivity computation. The impact of forcing in those two applications is discussed in sections 3 and 4. In section 5, conclusions and some perspectives for future use of model forcing are presented.

## 2. FORCING LINEAR MODELS: TWO APPLICATIONS

Suppose an operational NWP model can be written in the following form:

$$d\mathbf{x}/dt = G(\mathbf{x}). \quad (4)$$

The sensitive dependence on initial conditions  $\mathbf{x}(0)$  of Eq. (4) is of particular concern for operational weather centres. Small differences in the analysis  $\mathbf{x}(0)$  may result in entirely different forecasts. Therefore, knowledge about fast-growing perturbations with respect to the analysis is of great importance. One approach to finding such perturbations, and which has been adopted at the ECMWF, is to compute so-called singular vectors (SVs) of the associated tangent linear system of Eq. (4). Perturbations based on SVs can then be used in ensemble forecasting to inform about the likelihood of different weather scenarios (Molteni *et al.* 1996; Buizza *et al.* 1998). Other approaches of designing an ensemble forecast system are described by, for example, Toth and Kalnay (1997) and Houtekamer *et al.* (1996).

SVs provide an efficient tool to search for fast-growing perturbations of the analysis. It is even possible to define initial perturbations which are consistent with analysis-error statistics. This is of particular interest for predictability studies and it requires (see below for SV definition) an initial norm based on an estimate of the analysis-error covariance matrix. The Hessian or second derivative of the four-dimensional variation (4D-Var) cost function can be used to define such an initial norm. The final norm is less crucial and may depend on the meteorological phenomenon one is interested in (Ehrendorfer and Tribbia 1997; Barkmeijer *et al.* 1998; Palmer *et al.* 1998).

In addition to fast-growing perturbations of the analysis such as SVs, the forecast quality will also depend on the model formulation. Various components of operational forecast models, such as the parametrization of physical processes or the form of external forcing terms, allow for a certain degree of uncertainty. Suitable initial perturbations may compensate for certain model deficiencies and vice versa and ideally one would like to address the relative importance of both sources of forecast error. Harrison *et al.* (1999) and Evans *et al.* (2000) studied ensembles comprising members using the ECMWF and United Kingdom Meteorological Office (UKMO) model and analyses. The inclusion of either a second model or a second analysis improved the ensemble skill, but the greatest benefit resulted from using both models and analyses. Richardson (2001) found that especially the use of different operational analyses was beneficial for defining an ensemble strategy; the additional benefits of including different models was less clear.

In this paper, we adopt a simple approach to account for forecast error attributable to model error. We assume that the possible shortcomings in the model formulation can be described by a perturbation  $\mathbf{f}$  of the model tendencies, whose spatial pattern is kept constant in time. In other words, the linear evolution of a perturbation  $\varepsilon$  satisfies:

$$d\varepsilon/dt = \mathbf{L}\varepsilon + \mathbf{f}, \quad (5)$$

where  $\mathbf{L}$  denotes the time-dependent Jacobian of  $G$  evaluated along a solution of Eq. (4). Model tendency perturbations, usually of stochastic nature, are a familiar tool in various applications to describe unpredictable small-scale variability (e.g. Hasselman 1976;

DelSole and Farrell 1995; Moore and Kleeman 1999; Buizza *et al.* 1999; Vannitsen and Toth 2002). Solutions of Eq. (5) take the form:

$$\varepsilon(T) = \mathbf{M}(0, T)\varepsilon(0) + \int_0^T \mathbf{M}(s, T)\mathbf{f} ds, \quad (6)$$

where  $\mathbf{M}(s, T)$  is the propagator from time  $s$  to time  $T$  of Eq. (5) without forcing:  $\mathbf{f} = 0$ . The vector  $\mathbf{M}(0, T)\mathbf{y}$  is obtained by integrating Eq. (5) with  $\mathbf{f} = 0$  from time  $t = 0$  to time  $t = T$  starting with an arbitrary initial condition  $\mathbf{y}$ . In the following, we set the integration (or optimization) time to 48 hours and simplify the notation accordingly. SVs are usually characterized as structures that maximize the ratio between norms at initial and optimization time, as given by:

$$\frac{\langle \mathbf{P}\mathbf{x}, \mathbf{C}_1\mathbf{P}\mathbf{x} \rangle}{\langle \mathbf{x}, \mathbf{C}_0\mathbf{x} \rangle}. \quad (7)$$

Here  $\langle \cdot, \cdot \rangle$  denotes the Euclidean inner product  $\langle \mathbf{x}, \mathbf{y} \rangle = \sum \mathbf{x}_i \mathbf{y}_i$ . The operator  $\mathbf{P}$  is a projection operator that sets a vector to zero outside a given domain. The positive definite and symmetric operators  $\mathbf{C}_0$  and  $\mathbf{C}_1$  define a norm at initial and optimization time. The first singular vector, SV1, maximizes the ratio in Eq. (7), the second, SV2, maximizes this ratio in the subspace  $\mathbf{C}_0$ -orthogonal to SV1, and so forth. Thus, the SVs  $\mathbf{x}$  define a  $\mathbf{C}_0$ -orthogonal set at initial time. The evolved SVs  $\mathbf{M}\mathbf{x}$  form a  $\mathbf{C}_1$ -orthogonal set at optimization time in the projection domain defined by  $\mathbf{P}$ . Alternatively, these SVs are solutions of the following generalized eigenvalue problem

$$\mathbf{M}^* \mathbf{P}^* \mathbf{C}_1 \mathbf{P} \mathbf{M} \mathbf{x} = \lambda \mathbf{C}_0 \mathbf{x}. \quad (8)$$

The adjoint operators  $\mathbf{M}^*$  and  $\mathbf{P}^*$  are defined with respect to the Euclidean inner product. In the following,  $\mathbf{P}$  denotes a projection operator onto the northern hemisphere (NH) extratropics (30°N–90°N) and  $\mathbf{C}_0$  and  $\mathbf{C}_1$  are identical diagonal operators with total energy weights on the diagonal. The associated inner product reads as:

$$\begin{aligned} \langle \mathbf{x}, \mathbf{C}_0 \mathbf{y} \rangle = & \frac{1}{2} \int_{\eta=0}^1 \int_{\Sigma} (\nabla \Delta^{-1} \zeta_x \cdot \nabla \Delta^{-1} \zeta_y + \nabla \Delta^{-1} D_x \cdot \nabla \Delta^{-1} D_y) \\ & + \frac{c_p}{T_r} T_x T_y d\Sigma \left( \frac{\partial p}{\partial \eta} \right) d\eta + \frac{1}{2} \int_{\Sigma} R_d T_r P_r \ln \pi_x \cdot \ln \pi_y d\Sigma \end{aligned} \quad (9)$$

with  $(\zeta_x, D_x, T_x, \ln \pi_x)$  being the vorticity, divergence, temperature, and logarithm of the surface pressure components of the state vector  $\mathbf{x}$ , and  $c_p$  is the specific heat of dry air at constant pressure,  $p(\eta)$  the pressure at  $\eta$ -levels (0 = surface and 1 = top of atmosphere),  $R_d$  is the gas constant for dry air,  $T_r = 300$  K is a reference temperature, and  $P_r = 800$  hPa is a reference pressure. For this choice of  $\mathbf{C}_0$ , Eq. (8) can be readily written as a regular eigenvalue problem. First by multiplying both sides of Eq. (8) to the left by  $\mathbf{C}_0^{-\frac{1}{2}}$ :

$$\mathbf{C}_0^{-\frac{1}{2}} \mathbf{M}^* \mathbf{P}^* \mathbf{C}_1 \mathbf{P} \mathbf{M} \mathbf{x} = \lambda \mathbf{C}_0^{\frac{1}{2}} \mathbf{x} \quad (10)$$

and then by observing that

$$\begin{aligned} \mathbf{C}_0^{-\frac{1}{2}} \mathbf{M}^* \mathbf{P}^* \mathbf{C}_1 \mathbf{P} \mathbf{M} \mathbf{x} &= \mathbf{C}_0^{-\frac{1}{2}} \mathbf{M}^* \mathbf{P}^* \mathbf{C}_1 \mathbf{P} \mathbf{M} (\mathbf{C}_0^{-\frac{1}{2}} \mathbf{C}_0^{\frac{1}{2}} \mathbf{x}) \\ &= \mathbf{C}_0^{-\frac{1}{2}} \mathbf{M}^* \mathbf{P}^* \mathbf{C}_1 \mathbf{P} \mathbf{M} \mathbf{C}_0^{-\frac{1}{2}} (\mathbf{C}_0^{\frac{1}{2}} \mathbf{x}). \end{aligned} \quad (11)$$

Combining Eqs. (10) and (11) and writing  $\mathbf{v} = \mathbf{C}_0^{-\frac{1}{2}} \mathbf{x}$  results in

$$\mathbf{C}_0^{-\frac{1}{2}} \mathbf{M}^* \mathbf{P}^* \mathbf{C}_1 \mathbf{P} \mathbf{M} \mathbf{C}_0^{-\frac{1}{2}} \mathbf{v} = \lambda \mathbf{v}.$$

This is a symmetric eigenvalue problem suitable for the Lanczos algorithm (Parlett 1980), even when the involved operators are not known explicitly.

(a) *Forcing singular vectors*

Forcing singular vectors (FSVs) can be defined analogously to initial SVs. Instead of searching for  $\varepsilon(0)$  which yield large perturbation growth we are interested in structures,  $\mathbf{f}$ , with  $\varepsilon(0) = 0$ , which will produce large  $\varepsilon(T)$  (in some norm) as defined by Eq. (6). Ideally, one would like to constrain  $\mathbf{f}$  with a norm that reflects in some manner the uncertainty in model physics tendencies, as initial SVs can be defined with an initial norm that corresponds to analysis uncertainty (e.g. Barkmeijer *et al.* 1998). In this paper, both  $\mathbf{f}$  and its response  $\varepsilon(T)$  are measured in terms of total energy  $\mathbf{E}$ . As such the defining norms are the same as used for initial SVs. We have no evidence that such an energy norm reflects the uncertainty in the model physics. By writing  $\mathbf{E}$  for the operators  $\mathbf{C}_0$  and  $\mathbf{C}_1$ , FSVs  $\mathbf{f}$  satisfy the following eigenvalue problem:

$$\mathbf{E}^{-\frac{1}{2}} \mathcal{M}^* \mathbf{P}^* \mathbf{E} \mathbf{P} \mathcal{M} \mathbf{E}^{-\frac{1}{2}} \mathbf{f} = \lambda \mathbf{f} \quad \text{with} \quad \mathcal{M} = \int_0^T \mathbf{M}(s, T) ds. \quad (12)$$

For an arbitrary forcing  $\mathbf{f}$ , the vector  $\mathbf{y} = \mathcal{M}\mathbf{f}$  is simply determined by integrating Eq. (5) to time  $t = T$  with initial condition  $\varepsilon(0) = 0$ . To derive the adjoint of  $\mathcal{M}$  it is instructive to write Eq. (5) in the form of a  $2 \times 2$ -matrix system:

$$\frac{d}{dt} \begin{pmatrix} \varepsilon \\ \mathbf{f} \end{pmatrix} = \begin{pmatrix} \mathbf{L} & \mathbf{I} \\ \mathbf{O} & \mathbf{O} \end{pmatrix} \begin{pmatrix} \varepsilon \\ \mathbf{f} \end{pmatrix}, \quad (13)$$

where  $\mathbf{I}$  and  $\mathbf{O}$  are the identity and zero operator respectively. The adjoint of Eq. (13) reads as:

$$-\frac{d}{dt} \begin{pmatrix} \hat{\varepsilon} \\ \hat{\mathbf{f}} \end{pmatrix} = \begin{pmatrix} \mathbf{L}^* & \mathbf{O} \\ \mathbf{I} & \mathbf{O} \end{pmatrix} \begin{pmatrix} \hat{\varepsilon} \\ \hat{\mathbf{f}} \end{pmatrix}. \quad (14)$$

By writing the above system again as coupled system

$$-\frac{d}{dt} \hat{\varepsilon} = \mathbf{L}^* \hat{\varepsilon} \quad (15)$$

$$-\frac{d}{dt} \hat{\mathbf{f}} = \hat{\varepsilon} \quad (16)$$

it follows how to determine  $\mathcal{M}^* \mathbf{y}$  for a given input vector  $\mathbf{y}$ :

1. Integrate the regular adjoint model as given by Eq. (15) backward from time  $t = T$  to time  $t = 0$  with  $\hat{\varepsilon}(T) = \mathbf{y}$ .
2. Integrate Eq. (16) backward in time from time  $t = T$  using the intermediate fields of the adjoint integration (15) as tendencies for the corresponding time step and  $\hat{\mathbf{f}}(T) = 0$ . Integrating to time  $t = 0$  yields  $\mathcal{M}^* \mathbf{y} = \hat{\mathbf{f}}(0)$ .

An alternative procedure to evaluate  $\mathcal{M}^*$  was derived by D'Andrea and Vautard (2000). Observe that the above two steps 1 and 2 can easily be performed simultaneously and that therefore the computational costs for determining FSVs is the same as for

initial SVs. In fact, allowing the forcing  $\mathbf{f}$  in Eq. (5) only to act for the first time step results in FSVs that are equivalent to SVs. A special case is where the basic state, required to run the linear models, is constant in time. Instead of applying the above scheme,  $\mathcal{M}^*$  can also be obtained by integrating a forced adjoint equation backward in time, similarly to Eq. (5) for computing  $\mathcal{M}$ .

(b) *Forced sensitivity calculations*

In the sensitivity calculation, operational at the ECMWF since 1995 (Rabier *et al.* 1996; Klinker *et al.* 1998), the goal is to find a posteriori an analysis perturbation that results in an improved forecast. The same approach which was followed to define FSVs can also be applied to such a sensitivity calculation. That is, instead of searching for analysis perturbations that improve the forecast, possibly by reducing both analysis and model errors, one searches for tendency perturbations that improve the forecast. Central in the sensitivity calculation is the minimization of a cost function of the form:

$$J(\varepsilon) = \frac{1}{2}(\mathbf{M}\varepsilon - \mathbf{z})^T \mathbf{P}^T \mathbf{C}_1 \mathbf{P}(\mathbf{M}\varepsilon - \mathbf{z}), \quad (17)$$

where the operators  $\mathbf{P}$  and  $\mathbf{M}$  are as in the SV computation, i.e. a projection operator and the propagator of the linear model respectively, and the superscript T stands for transpose of an operator. The field  $\mathbf{z}$  is the 2-day forecast error, which the linear integrated analysis perturbation  $\mathbf{M}\varepsilon$  tries to decrease. Note that the same sensitivity procedure can also be used to produce prescribed flow regimes in the forecast with suitable perturbations (Oortwijn and Barkmeijer 1995; Corti and Palmer 1997).

The gradient used in the minimization procedure of  $J$  depends on the constraint on  $\varepsilon$ , here  $\langle \mathbf{C}_0 \varepsilon, \varepsilon \rangle$  is constant, and is given by:

$$\nabla J = \mathbf{C}_0^{-1} \mathbf{M}^* \mathbf{P}^* \mathbf{C}_1 \mathbf{P}(\mathbf{M}\varepsilon - \mathbf{z}). \quad (18)$$

Using a standard quasi-Newton minimization package, the cost function  $J$  is minimized. Typically three iterations in the minimization procedure suffice to achieve a reasonable reduction of the cost function. As is clear from Eq. (18), the final analysis perturbation (commonly called key analysis error) strongly depends on the initial inner product induced by  $\mathbf{C}_0$  (see, also, Klinker *et al.* (1998)).

In the *forced* sensitivity calculation, the only way to decrease the cost function is by applying time independent tendency perturbations. This means that the linear model for evolving perturbations is given by Eq. (5), and during each iteration in the minimization process Eq. (5) is integrated with  $\varepsilon(0) = 0$  and with the forcing  $\mathbf{f}$  found in the previous iteration. The gradient direction used in the minimization during each iteration is given by

$$\mathbf{C}_0^{-1} \mathcal{M}^* \mathbf{P}^* \mathbf{C}_1 \mathbf{P}(\mathcal{M}\varepsilon - \mathbf{z}), \quad (19)$$

where  $\mathcal{M}$  and  $\mathcal{M}^*$  are as defined in section 2(a). In the experiments described below  $\mathbf{C}_0$  and  $\mathbf{C}_1$  are identical and equal to the total energy operator  $\mathbf{E}$ .

### 3. COMPARISON OF INITIAL AND FORCING SINGULAR VECTORS

For two weeks, 1–7 January 2000 and 1–7 July 2000, daily initial and forcing SVs have been computed starting at 1200 UTC and with an optimization time of 48 hours. As already pointed out, perturbation growth is measured in terms of the total energy inner product (see Eq. (9)) and consequently FSVs are solutions of Eq. (12). Initial SVs satisfy a similar equation, but with  $\mathcal{M}$  replaced by the usual propagator  $\mathbf{M}$ .

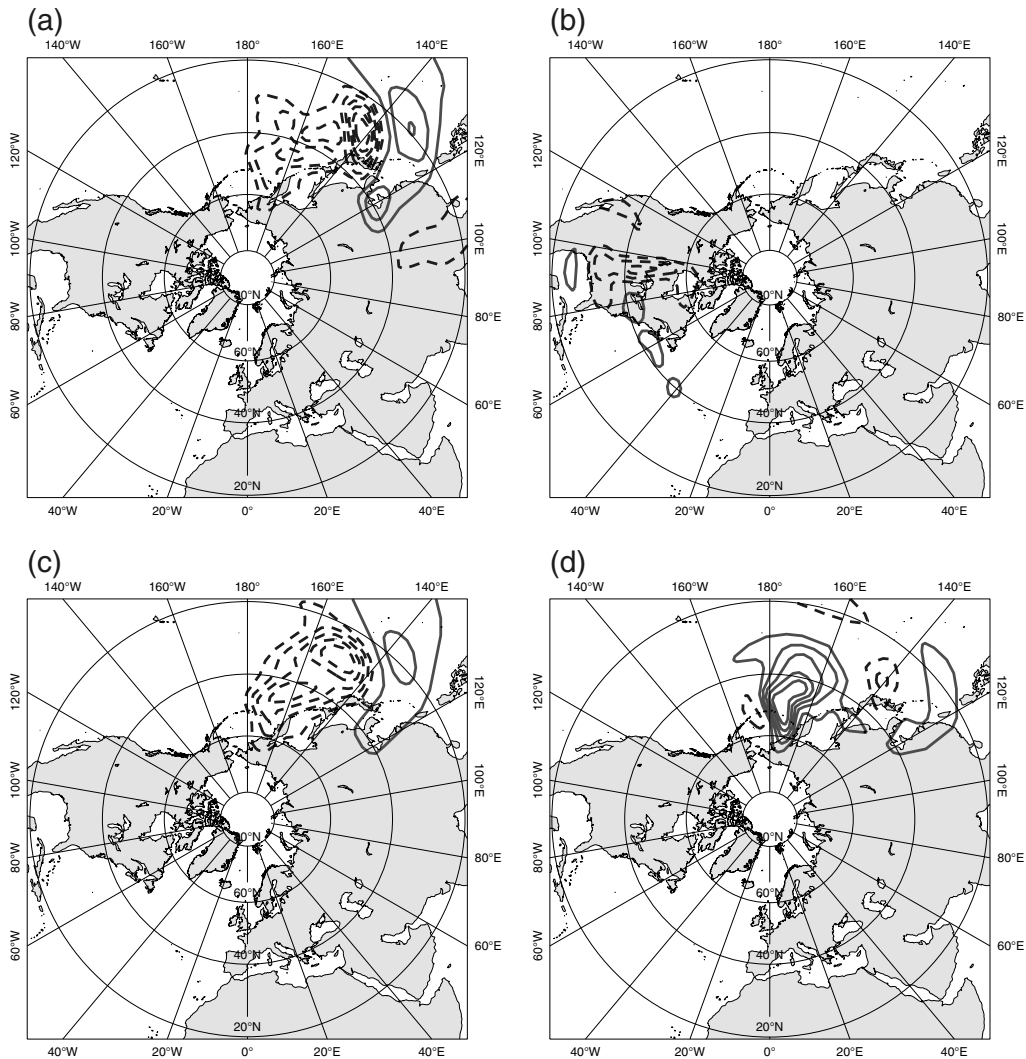


Figure 1. Stream-function fields around 500 hPa for the two leading (a) and (b) singular vectors and (c) and (d) forcing singular vectors (multiplied by time factor 1 s) starting from 1200 UTC 3 January 2000. Contour interval is  $0.004 \text{ m}^2\text{s}^{-1}$  with negative values shown by dashed lines.

Both computations are performed with a horizontal resolution T42 and a vertical resolution of 40 levels. The nonlinear trajectories required to run the linear models are produced by a low-resolution T42 version of the operational ECMWF forecast model. The linear models are used in their diabatic configuration and comprise linear versions of most of the important physics packages of the ECMWF forecast model (Mahfouf 1999).

An example of SVs and FSVs is shown in Fig. 1 for a calculation starting from 1200 UTC 3 January 2000. The two top and bottom panels show the stream-function fields of the leading two SVs and FSVs, respectively, at nearly 500 hPa. The leading SV and FSV are located in the same region, and the second FSV seems somewhat larger in scale. The latter will be confirmed below when the horizontal spectrum is considered (see Fig. 5). The occurrence of larger scale structures in FSVs is probably because only

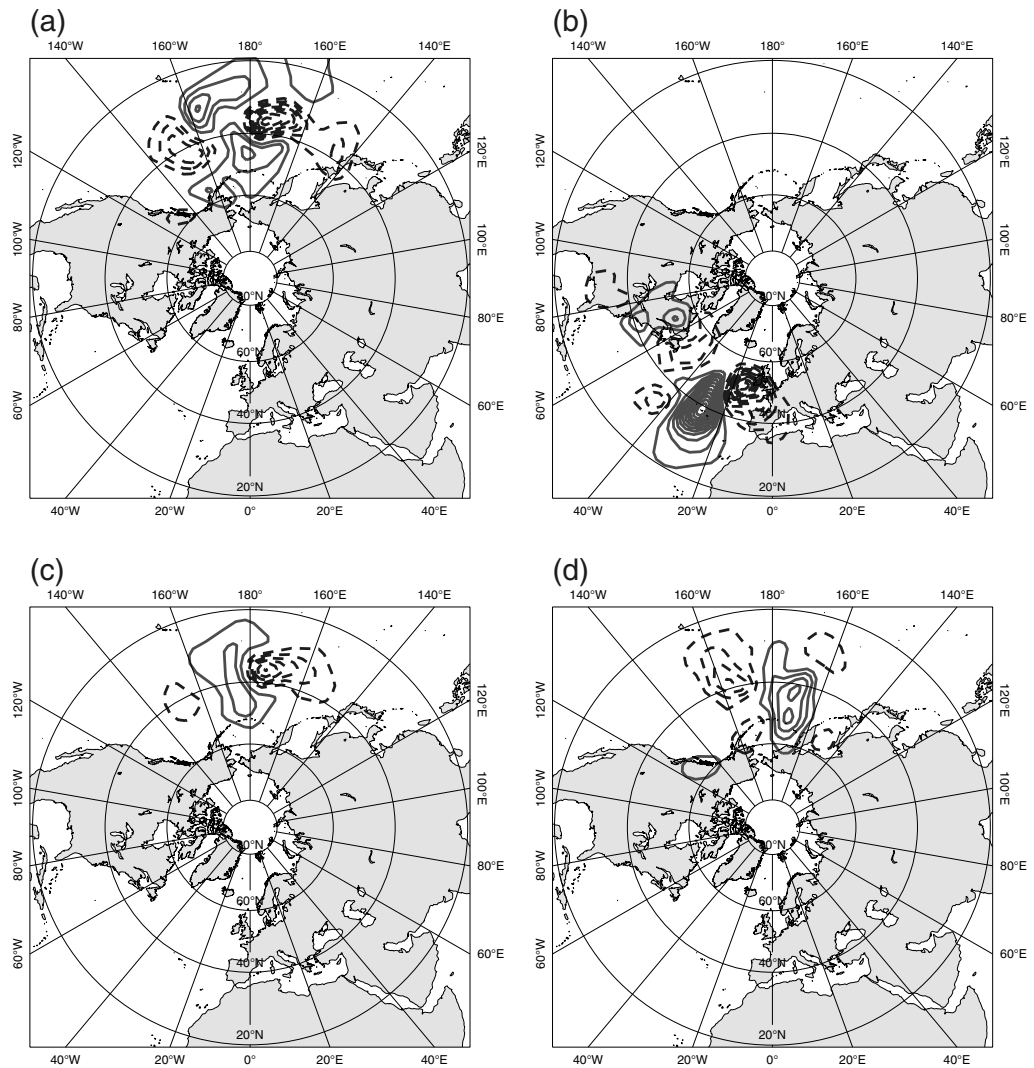


Figure 2. As Fig. 1, but the linear response after two days for (a) and (b) singular vectors and (c) and (d) forcing singular vectors. Contour interval in (a) and (b) is  $0.06 \text{ m}^2\text{s}^{-1}$  and in (c) and (d)  $4000 \text{ m}^2\text{s}^{-1}$ . Negative values are shown by dashed lines.

constant tendency perturbations are allowed during the optimization time. This means that an FSV contributes to perturbation growth during the entire optimization time (see Eq. (12)). In the forced sensitivity calculations also, large scale structures were observed (see Fig. 9(b)). The corresponding evolved vectors are shown in Fig. 2. Components of the second FSV display an almost *in situ* growth which is rarely seen for initial SVs. The latter feature is also noticeable in root-mean-square patterns given by the leading SVs or FSVs for the winter and summer cases. Figures 3 and 4 show for the seven winter and summer cases, respectively, root-mean-square stream-function fields based on the ten leading SVs or FSVs and their associated evolved vectors. Each vector is weighted by a factor  $\sigma_i / \sum_{k=1}^{10} \sigma_k$ , with  $\sigma_i$  the singular value corresponding to vector  $i$ . In addition to regions where initial SVs are located, it appears

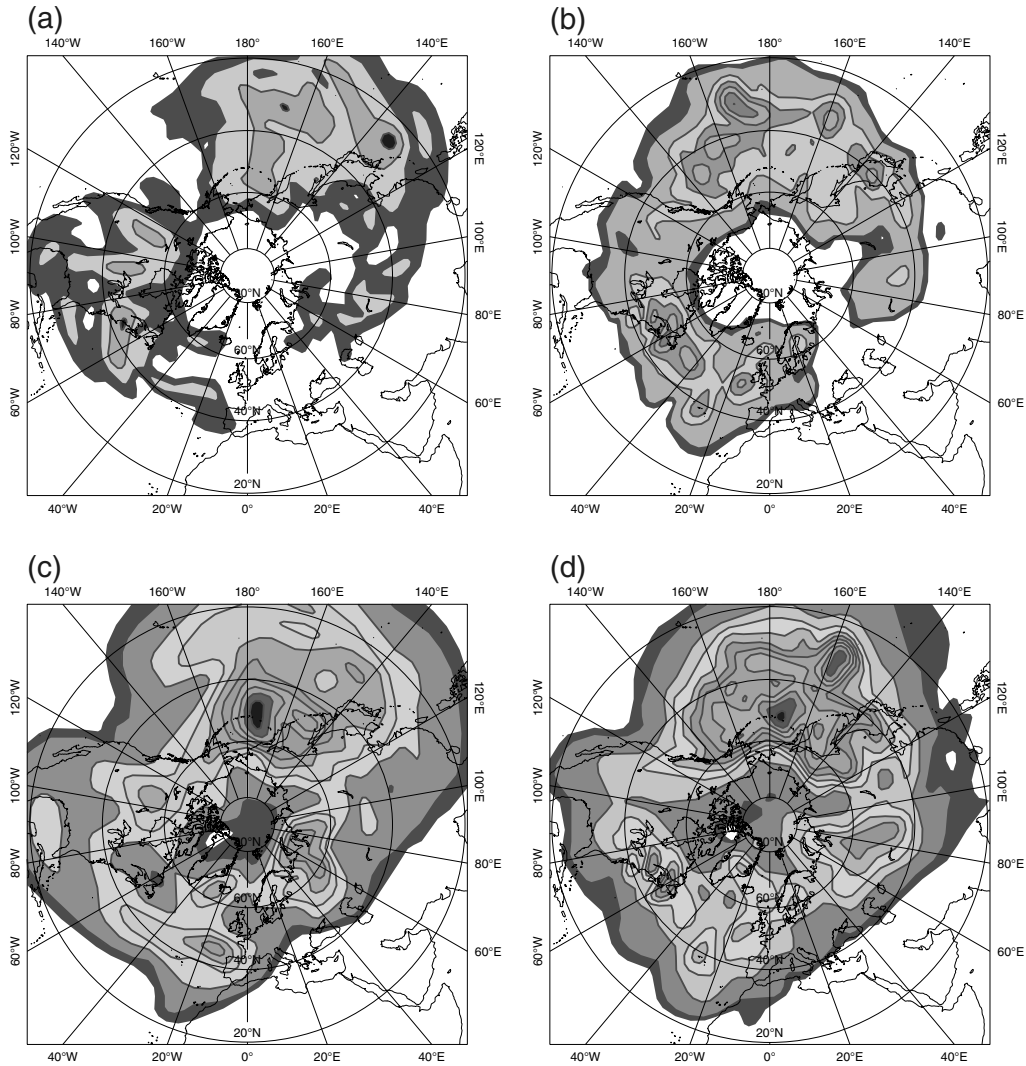


Figure 3. Root-mean-square stream-function fields around 500 hPa for the seven winter cases (see text) and based on the ten leading (a) singular vectors (SVs), (b) evolved SVs, (c) forcing singular vectors (FSVs) (multiplied by time factor 1 s) and (d) evolved FSVs and weighted by the corresponding singular value. Contour interval in (a) and (c) is  $0.00035 \text{ m}^2\text{s}^{-1}$ , (b)  $0.01 \text{ m}^2\text{s}^{-1}$  and (d)  $250 \text{ m}^2\text{s}^{-1}$ . The shading has no significance.

as though the FSVs also seem to favour the area west of the Iberian Peninsula and between  $40^\circ\text{E}$ – $100^\circ\text{E}$  and  $50^\circ\text{N}$ – $80^\circ\text{N}$ . The response  $\mathcal{M}\mathbf{f}$  of FSVs  $\mathbf{f}$  initiating from those areas show only small propagation.

To quantify possible differences between SVs and FSVs, total energy spectra and vertical distributions of total energy were determined as shown in Figs. 5 and 6. The average was taken over the leading 25 SVs and FSVs and associated evolved vectors for the seven winter and summer cases. Note that the evolved forcing singular vector  $\mathbf{f}$  is given by  $\mathcal{M}\mathbf{f}$  and that SVs and FSVs are normalized with unit total energy norm.

The vertical distribution of total energy for SVs and FSVs and evolved vectors are quite similar. The maximum amplitude for SVs and FSVs is mainly in the potential

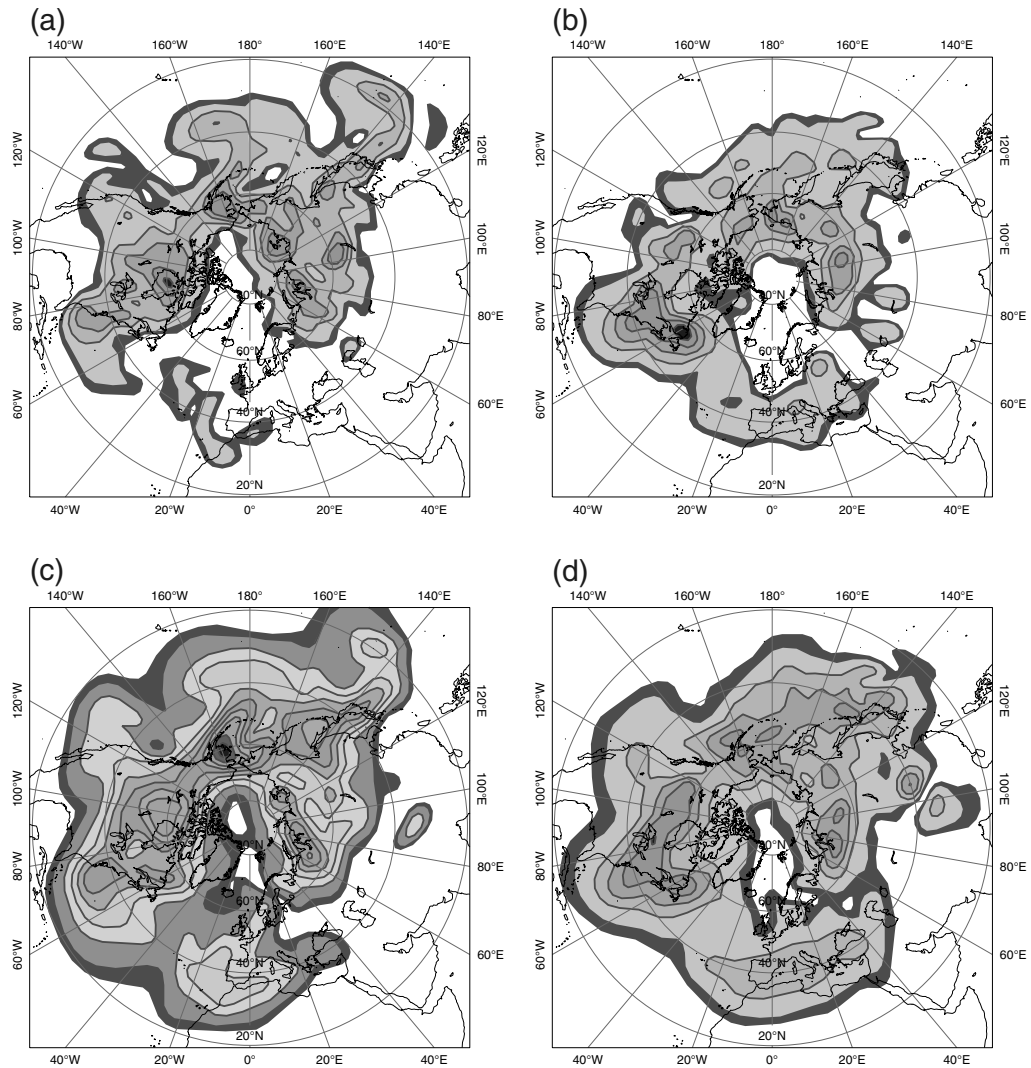


Figure 4. Same as Fig. 3 but for the seven summer cases (see text). Contour interval in (a) and (c) is  $0.00035 \text{ m}^2 \text{ s}^{-1}$ , (b)  $0.006 \text{ m}^2 \text{ s}^{-1}$  and (d)  $220 \text{ m}^2 \text{ s}^{-1}$ .

energy component around 600 hPa, and the evolved vectors show an upward perturbation growth with maximum amplitude around 300 hPa, dominated by the kinetic energy component. However, the horizontal spectra differ considerably. The upscale cascade of perturbation growth that is clearly visible in the SV spectra is absent for FSVs. There is more energy at the larger scales for FSVs with maximum amplitudes around wave number 12 and 15 in winter and summer, respectively. The evolved vectors have maximum amplitude around wave number 14. The difference in perturbation growth for SVs between the winter and summer period is clearly indicated by the area under the curves for the evolved vectors; for FSVs the seasonal dependence of perturbation growth is much smaller. Figure 7(a) presents the square root of the leading singular value for each winter and summer case. Note that the FSV singular values are scaled by a factor  $1/(\text{OT})^2$  with OT the optimization time (48 hours) in seconds. This was done because

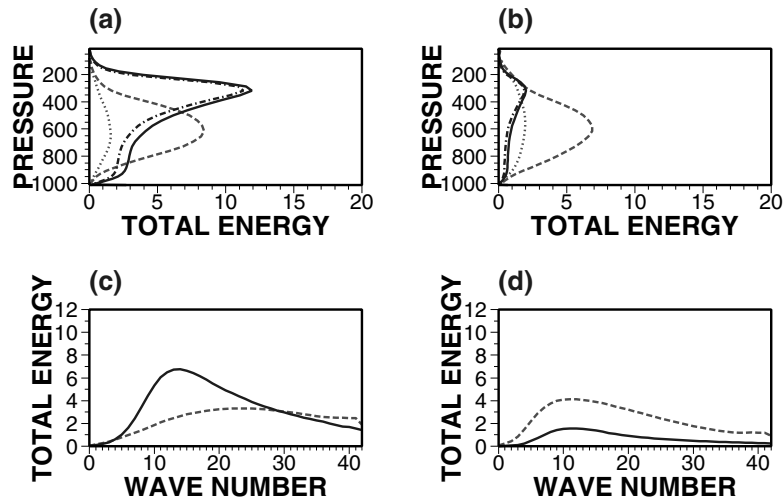


Figure 5. Vertical energy profiles for (a) singular vectors (SVs) and (b) forcing singular vectors (FSVs) and horizontal total energy spectrum for (c) SVs and (d) FSVs averaged over the seven winter cases (see text). Total (kinetic) energy for SVs and FSVs is plotted with a dashed (dotted) line. Total (kinetic) energy results for evolved vectors are plotted in full (dashed-dotted) lines. Values for SVs and FSVs are multiplied by a factor of 100; values for evolved FSVs are multiplied by  $10^{-8}$ .

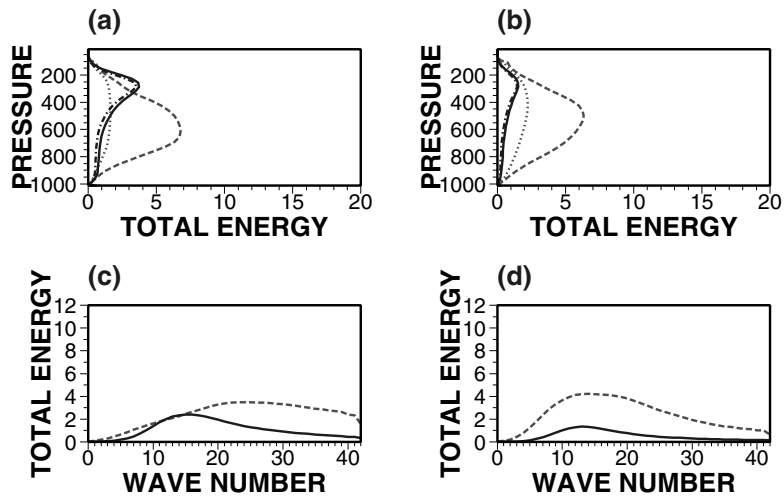


Figure 6. Same as Fig. 5 but for the seven summer cases (see text).

a forcing singular vector  $\mathbf{f}$  invariant under  $\mathbf{M}$ , i.e.  $\mathbf{M}(0, s)\mathbf{f} = \mathbf{f}$  for  $0 \leq s \leq OT$ , would yield a singular value of  $(OT)^2$ . The variability of leading singular value is quite similar for SVs and FSVs in winter; for the summer cases the FSVs singular values display less variability. In Fig. 7(b) the singular value spectrum for the leading 25 SVs and FSVs is given averaged over the summer and winter cases. Again the small seasonal dependence of FSV values is noticeable.

Another method to reveal differences between SVs and FSVs is to use a similarity index (Buizza *et al.* 1998) which measures how parallel are the subspaces spanned by the leading SVs and FSVs. Values of the similarity index vary from 0 to 1, and increasing

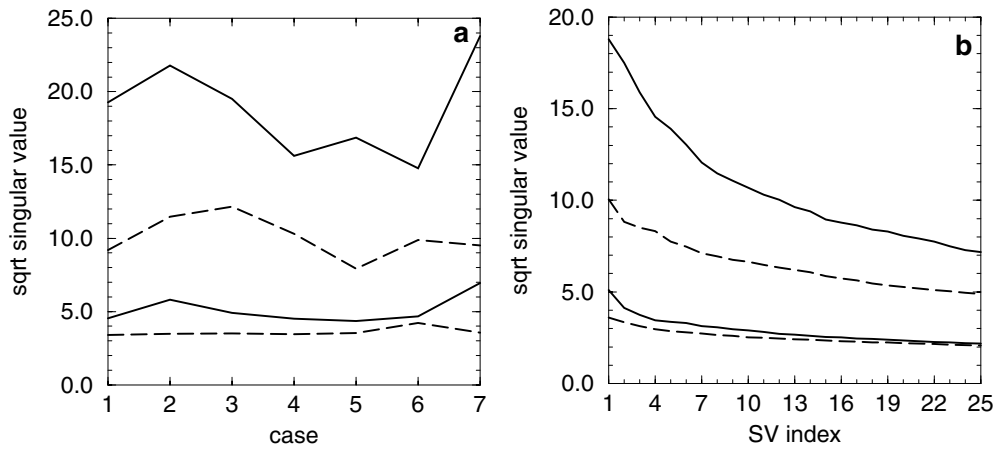


Figure 7. (a) The top two curves show the square root of the leading singular vectors (SVs) singular values for the seven winter (full line) and summer (dashed line) cases; the bottom two curves show scaled results for forcing singular vectors (FSVs) (see text for more details). (b) Leading 25 square-root singular values (averaged) for the winter (top two curves) and summer cases (bottom two curves). Full (dashed) lines denote SV (FSV) values.

TABLE 1. SIMILARITY INDICES BETWEEN UNSTABLE SUBSPACES SPANNED BY THE LEADING 25 SINGULAR VECTORS (SVs) AND FORCING SINGULAR VECTORS (FSVs) AND SPANNED BY THE ASSOCIATED EVOLVED VECTORS FOR THE WINTER AND SUMMER 2000 CASES. ALSO FOR EACH PERIOD SIMILARITY INDICES BETWEEN CONSECUTIVE UNSTABLE SUBSPACES ARE GIVEN FOR SVs AND FSVs.

Winter 2000 cases					Summer 2000 cases				
	SV-FSV	Evolved	SV	FSV		SV-FSV	Evolved	SV	FSV
1 January	0.29	0.61	0.10	0.24	1 July	0.34	0.57	0.15	0.40
2 January	0.28	0.58	0.13	0.25	2 July	0.29	0.52	0.20	0.39
3 January	0.26	0.55	0.09	0.22	3 July	0.33	0.60	0.15	0.37
4 January	0.25	0.57	0.07	0.20	4 July	0.36	0.59	0.18	0.42
5 January	0.22	0.51	0.06	0.27	5 July	0.39	0.69	0.17	0.37
6 January	0.24	0.48	0.08	0.31	6 July	0.38	0.71	0.12	0.33
7 January	0.24	0.5			7 July	0.34	0.6		

values mean that the subspaces become more and more parallel. Table 1 gives for each of the seven winter and summer cases the similarity between the subspaces spanned by the leading 25 SVs or FSVs and their associated evolved vectors. It shows that both computations explore different unstable subspaces, yet describe similar subspaces at optimization time. For comparison, the similarity indices are given between consecutive (1-day difference) unstable subspaces for SVs and FSVs. Clearly, there is more similarity between consecutive unstable subspaces in summer than in winter both for SVs and FSVs. The special FSV property of being time independent during the optimization period probably introduces some memory of FSV computation started one day earlier, resulting in increased similarity indices.

Because the SV and FSV unstable subspaces are dissimilar, it is possible that the two sets of vectors describe different parts of the forecast error. To investigate this, the operational 2-day NH T42L40 forecast error  $e(48)$  was projected onto the 2-day linearly evolved SVs and FSVs for each of the seven winter and summer cases. In the projection, the leading 25 leading evolved vectors of type SV or FSV were used. Denote by  $\tilde{e}(48)$  the portion of the forecast error thus explained and the associated pseudo inverse error

TABLE 2. THE EXPLAINED PART OF 2-DAY NORTHERN HEMISPHERE FORECAST ERROR IN TERMS OF TOTAL ENERGY USING THE 25 LEADING SINGULAR VECTORS (SVs) OR FORCING SINGULAR VECTORS (FSVs)

Winter 2000 cases	SV	FSV	Summer 2000 cases	SV	FSV
1 January	0.22	0.24	1 July	0.13	0.18
2 January	0.22	0.19	2 July	0.08	0.08
3 January	0.13	0.14	3 July	0.19	0.16
4 January	0.22	0.25	4 July	0.14	0.13
5 January	0.16	0.16	5 July	0.14	0.13
6 January	0.13	0.14	6 July	0.1	0.12
7 January	0.1	0.15	7 July	0.15	0.15

(Gelaro *et al.* 1998) by  $\tilde{e}(0)$ :

$$\tilde{e}(48) = \sum_{i=1}^{25} a_i \mathbf{T}(\mathbf{SV}_i) = \mathbf{T}\tilde{e}(0) \quad (20)$$

where  $a_i$  is the projection coefficient associated with the  $i$ th evolved vector and  $\mathbf{T}$  can be either  $\mathbf{M}$ , the propagator of the tangent model, or  $\mathcal{M} = \int_0^{48\text{h}} \mathbf{M} ds$ . The percentage of the total energy of  $e(48)$  as explained by  $\tilde{e}(48)$  using SVs or FSVs is given in Table 2. Both types of vectors are able to describe nearly the same fraction of  $e(48)$  in terms of total energy.

Although, in general, the part of the forecast error described by SVs or FSVs is also spatially similar, regional differences may occur. Figure 8 shows the analysis or tendency perturbation  $\tilde{e}(0)$  based on SVs or FSVs, respectively and the associated  $\tilde{e}(48)$ , the projection onto the evolved SVs or FSVs of the 2-day 500 hPa geopotential height error for forecasts started from 1200 UTC 1 January 2000. The full 2-day forecast error is given in Fig. 8(e). Both analysis and tendency perturbation, as shown in Figs. 8(a) and (b), respectively, evolve to describe large parts of the forecast error in a similar manner (see Figs. 8(c) and (d)). However, there are also differences, notably between 40°E–80°E. Inspection of the leading 25 evolved SVs (results not shown here) reveals that all have only small amplitude in this area. It seems that tendency perturbations are more efficient in reducing the forecast error in this area. Of course, by increasing the number of SVs used in Eq. (20), this part of the forecast error will eventually be captured by the evolved SVs. It turns out that around 40–50 SVs are required to describe this regional forecast error to the same extent as the leading 25 FSVs.

#### 4. IMPACT OF FORCING ON SENSITIVITY CALCULATIONS

Sensitivity calculations were performed for a 7-day period: 24–30 October 2000. The models used in determining the cost function (Eq. (17)) and its gradient (Eq. (18)) had a horizontal resolution of T63, 60 levels in the vertical and were run in their diabatic configuration. The default sensitivity calculation seeks the analysis perturbation that yields the largest forecast-error reduction, by minimizing the cost function for a limited number of gradient computations. In the results shown here, six gradient computations were allowed and the forecast period was set to 2 days. The actual forecast error  $\mathbf{z}$  which has to be reduced in the minimization process is the difference between the T63L60 2-day forecast and the verifying operational ECMWF analysis truncated at T63 and projected onto the NH extratropics (30°N–90°N) by  $\mathbf{P}$ .

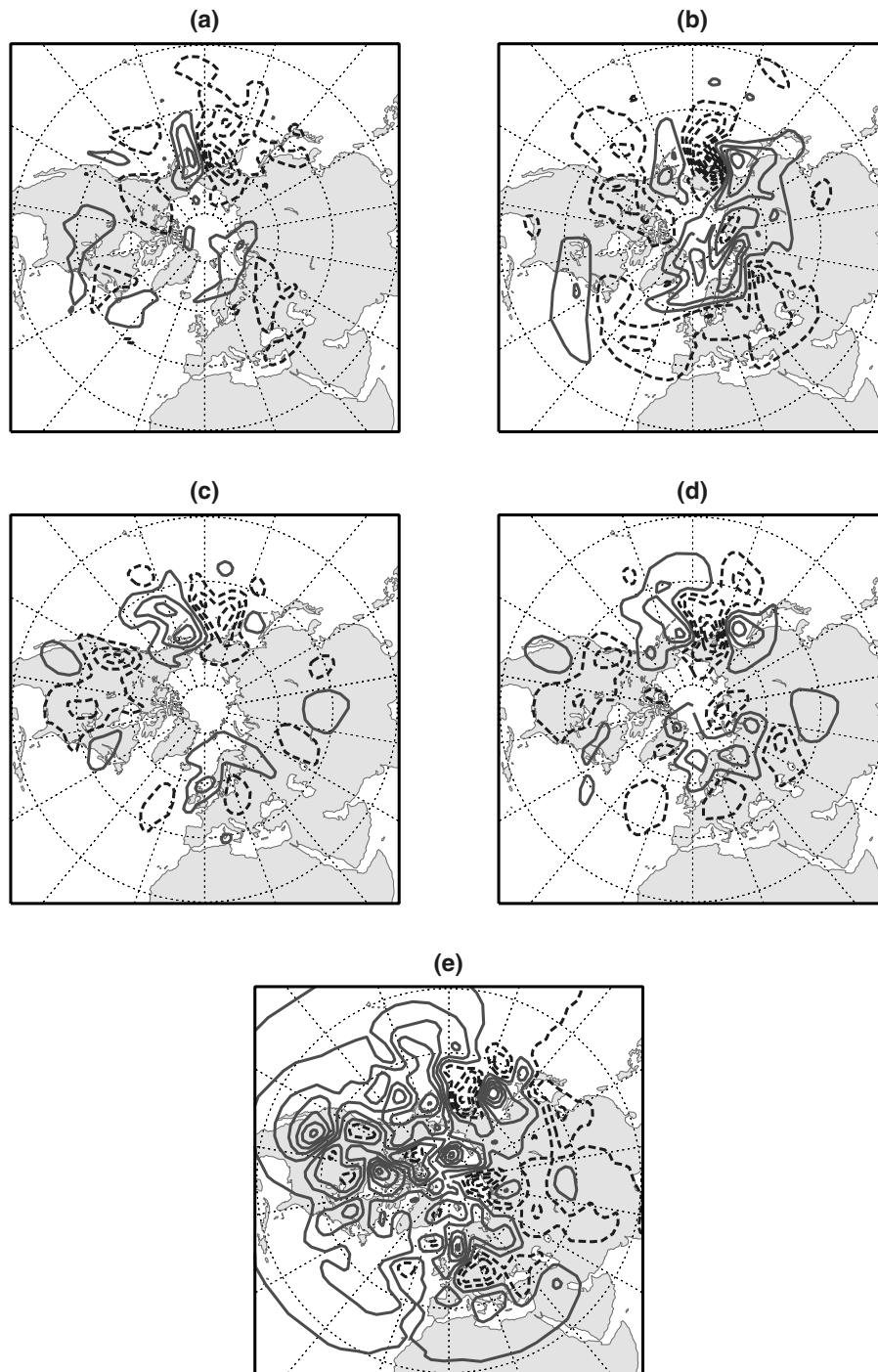


Figure 8. Pseudo inverse error  $\tilde{\epsilon}(0)$  (see text for more details) in geopotential height at 500 hPa for (a) singular vectors and (b) forcing singular vectors; (c) and (d) show corresponding  $\tilde{\epsilon}(48)$  and (e) 2-day geopotential height forecast error from 1200 UTC 1 January 2000. Contour interval in (a) is 1 m, (b)  $2.0 \times 10^{-5} \text{ m s}^{-1}$  and (c)–(e) 20 m, with negative values shown dashed.

TABLE 3. THE EXPLAINED FRACTION OF 2-DAY NORTHERN HEMISPHERE FORECAST ERROR MEASURED IN TERMS OF TOTAL ENERGY FOR DEFAULT AND FORCED SENSITIVITY COMPUTATIONS

Date (2000)	Default	Forced
24 October	0.19	0.45
25 October	0.42	0.62
26 October	0.34	0.57
27 October	0.36	0.59
28 October	0.41	0.60
29 October	0.41	0.59
30 October	0.29	0.53

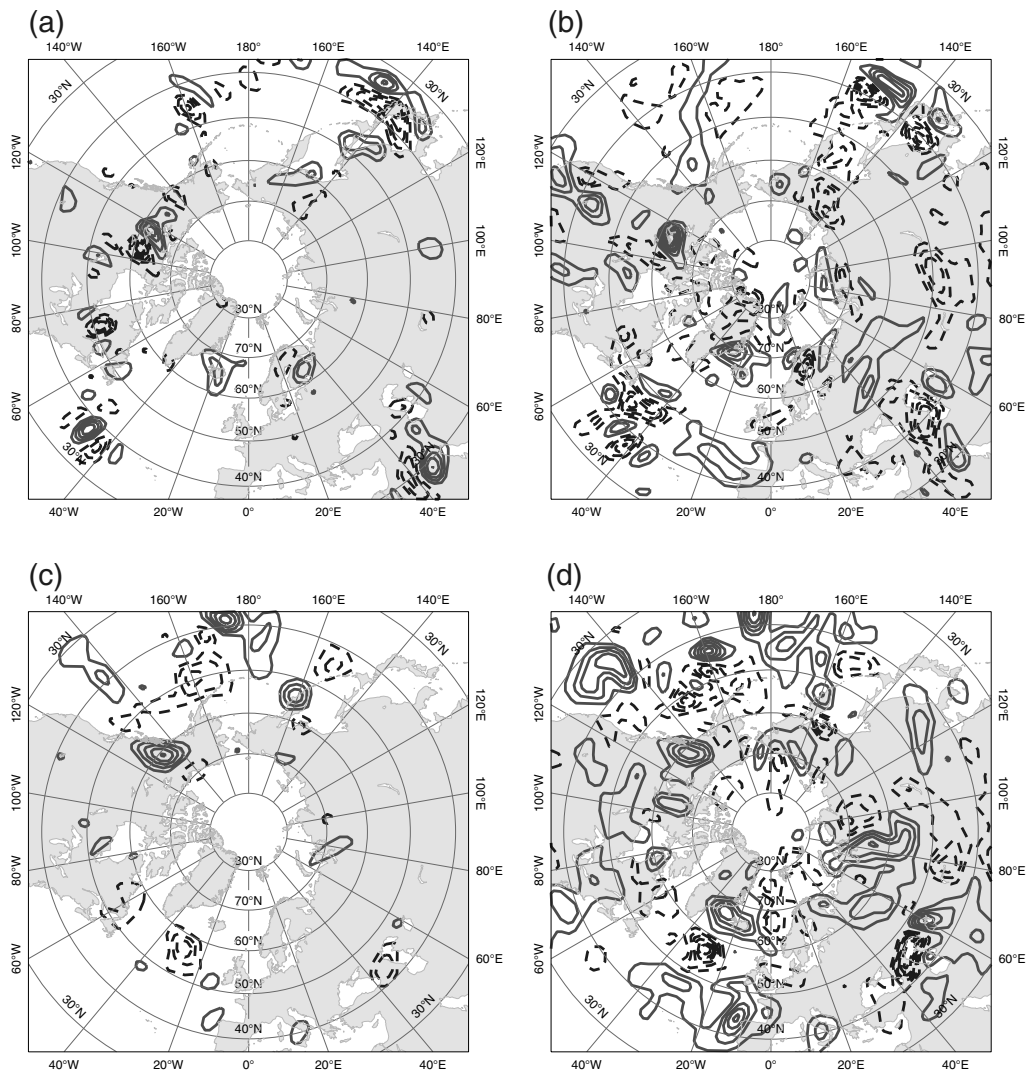


Figure 9. (a) and (b) Temperature perturbations at model level 44 (around 700 hPa) for 12 UTC 24 October 2000 after six iterations with the (a) default and (b) forced sensitivity calculation. (c) and (d) Corresponding linearly evolved temperature fields at model level 39 (around 500 hPa). Contour interval used in (a) is 0.1 K, (b)  $1.0 \times 10^{-5} \text{ K s}^{-1}$  and in (c) and (d) 1 K, with negative values shown dashed.

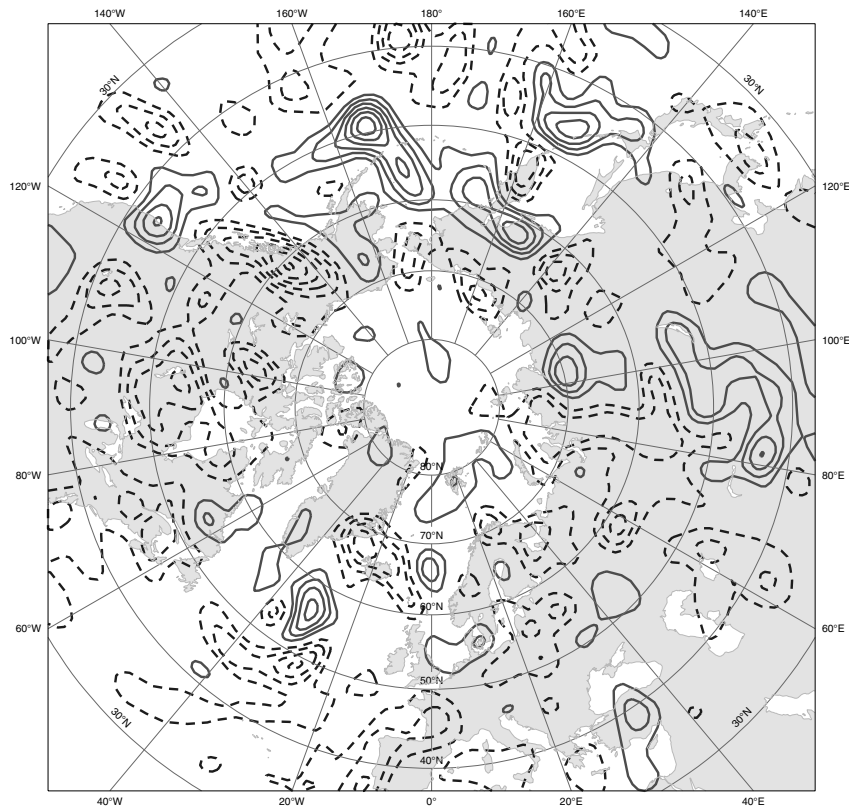


Figure 10. Two-day forecast error for temperature at model level 39 for the T63 forecast started from 1200 UTC 24 October 2000. Contour interval is 1 K with negative values shown dashed.

As explained in section 2(b), the same procedure of the default sensitivity calculation can be adapted to determine the model tendency perturbation  $\mathbf{f}$  which, given certain constraints such as the number of gradient computations, results in the greatest forecast-error reduction. Table 3 compares the reduction in the cost function after six iterations for the default and forced sensitivity calculations. Clearly, in each of the seven cases the tendency perturbations are better at reducing the forecast error than the so-called key analysis errors. The additional explained fraction of the total forecast error in terms of total energy is at least 20% more for the forced sensitivity calculation. Note that the tendency perturbation does not vary with time and is applied every time step during the integration. A trivial choice for a time-varying tendency perturbation  $\mathbf{f}(t)$  that would reduce the cost function to zero immediately would be to set  $\mathbf{f}(t) = 0$ , apart from the final time step when  $\mathbf{f}(t) = \mathbf{z}/\Delta t$ , with  $\mathbf{z}$  the 2-day forecast error and  $\Delta t$  the model time step. Such a forcing  $\mathbf{f}$  is, however, physically not realistic. The search for physically more acceptable time-varying forcing structures, for example by demanding some correlation in time, is beyond the scope of this paper. The necessary generalization of the procedure outlined in section 2(a) will be addressed in a follow-up study.

The perturbations determined by both sensitivity calculations are quite different from the forecast error that has to be corrected. The average correlation in terms of total energy between the forecast error and analysis or tendency perturbation is  $2.2 \times 10^{-3}$

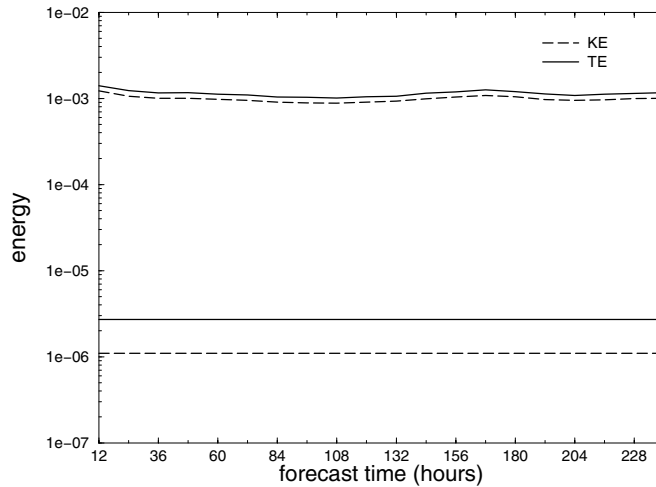


Figure 11. Average northern hemisphere (seven cases) total energy (TE) and kinetic energy (KE) of the full T63 model tendencies (upper lines) and of the forcing perturbations (lower lines) as functions of forecast time for 10-day forecasts every 12 hours.

TABLE 4. TOTAL ENERGY RATIO OF LINEAR AND NONLINEAR EVOLVED PERTURBATIONS FOR DEFAULT AND FORCED SENSITIVITY (AND THEIR CORRELATION)

Date (2000)	Default	Forced
24 October	1.69 (0.47)	1.43 (0.73)
25 October	1.82 (0.71)	1.34 (0.81)
26 October	1.82 (0.77)	1.34 (0.84)
27 October	1.84 (0.74)	1.36 (0.81)
28 October	1.72 (0.77)	1.34 (0.83)
29 October	2.06 (0.69)	1.44 (0.80)
30 October	1.69 (0.69)	1.36 (0.80)

and  $3.1 \times 10^{-3}$  for default and forcing sensitivity respectively. Figure 9 shows for 1200 UTC 24 October 2000 the analysis and tendency temperature perturbation at model level 44 (around 700 hPa) together with the associated linearly evolved temperature perturbation at level 39 (around 500 hPa) for the default and forced sensitivity calculation. The better reduction of the cost function in the case of the forcing calculation becomes apparent when the linearly evolved fields in Figs. 9(c) and (d) are compared with the actual T63 2-day forecast error (see Fig. 10). The forecast error over the Atlantic region, particularly to the west of the Iberian Peninsula is nicely captured by the forcing perturbation, as is the forecast error over the ( $60^{\circ}\text{E}$ – $100^{\circ}\text{E}$ ;  $20^{\circ}\text{N}$ – $60^{\circ}\text{N}$ ) region.

In order to have some understanding of the relative size of the tendency perturbations compared with the full tendencies, their amplitude over the NH was determined. The averaged NH total energy and its kinetic-energy component (cf. Fig. 5) of full and perturbation tendencies are plotted in Fig. 11 for 10-day forecasts every 12 hours.

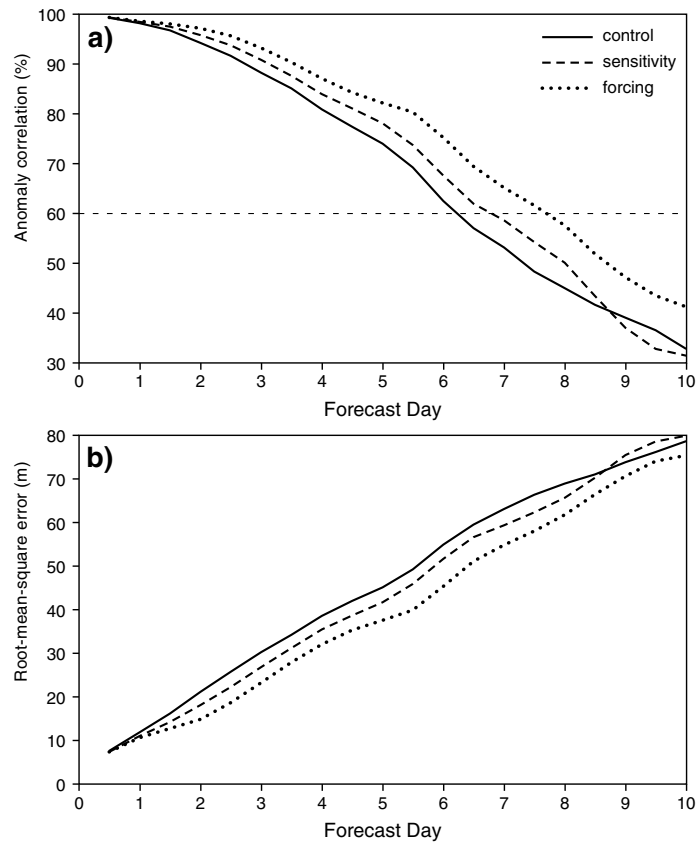


Figure 12. Average T63 forecast performance (seven cases) for northern hemisphere geopotential height in terms of (a) and (c) anomaly correlation and (b) and (d) root-mean-square error at (a) and (b) 1000 hPa and (c) and (d) 500 hPa. The lines in each panel represent unperturbed forecasts (full lines), with analysis perturbations (dashed lines) and tendency perturbations (dotted lines).

Most energy of the full model tendencies is in the kinetic-energy component of total energy; for forcing perturbations the potential-energy component is the largest. The latter agrees well with the energy distribution for FSVs (see Fig. 5). Although the magnitudes of the model tendencies and forcing perturbations are difficult to compare, it is clear from Fig. 11 that forcing perturbations are substantially smaller than model tendencies in terms of NH kinetic and potential energy (note the logarithmic scale). Another indication whether linearly computed tendency perturbations are sufficiently small is to consider how well linear and nonlinear integrated perturbations compare. Table 4 gives total energy correlations between linear and nonlinear 2-day integrated perturbations for default and forcing sensitivity and their total energy ratios. Clearly, the perturbations grow faster in the linear model as indicated by the larger-than-one total energy ratio. For most of the cases, the linear and nonlinear evolutions resemble each other quite well. This is, in particular, the case for forcing perturbations.

The average performance for geopotential height at 500 hPa of nonlinear forecasts using default and forcing perturbations is displayed in Fig. 12. The extent to which forecasts improve is in accordance with results obtained in a linear context such as the

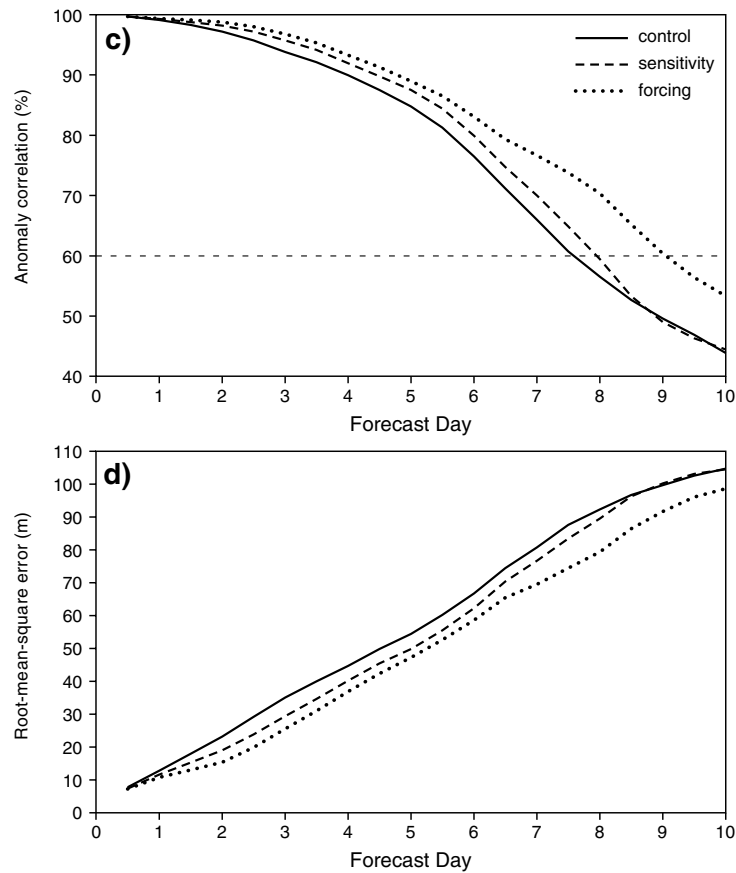


Figure 12. Continued.

cost-function reduction. Notice that although the forcing perturbation is applied during the entire forecast period it does not seem to have a deteriorating effect on the forecast performance after the optimization time of 2 days. Forecasts whereby the forcing is switched off after the optimization time show similar results (not shown). After the optimization time, the forcing perturbations have become sub-optimal, and they will probably have similar impact as random forcing perturbations, without necessarily having the capability to perturb the forecasts substantially.

To study the behaviour of forcing sensitivity also in summer, initial and forcing sensitivity computations were done for the period 1 May–8 June 2001 (39 cases). With the same configuration as the winter experiment we found basically the same performance as in winter. For example, a 19% more reduction of the cost function after six iterations in the case of forcing sensitivity (averaged over 39 cases). Figure 13 shows the impact on the 2-day systematic error for the initial and forcing sensitivity during this summer period. The systematic error was determined by taking the mean of all differences between the 2-day forecast and the verifying ECMWF analysis. Both sensitivity configurations are able to reduce systematic error but the reduction in the case of forcing sensitivity is much larger. The systematic error in the North Atlantic region has almost vanished, and over North America the systematic error has decreased

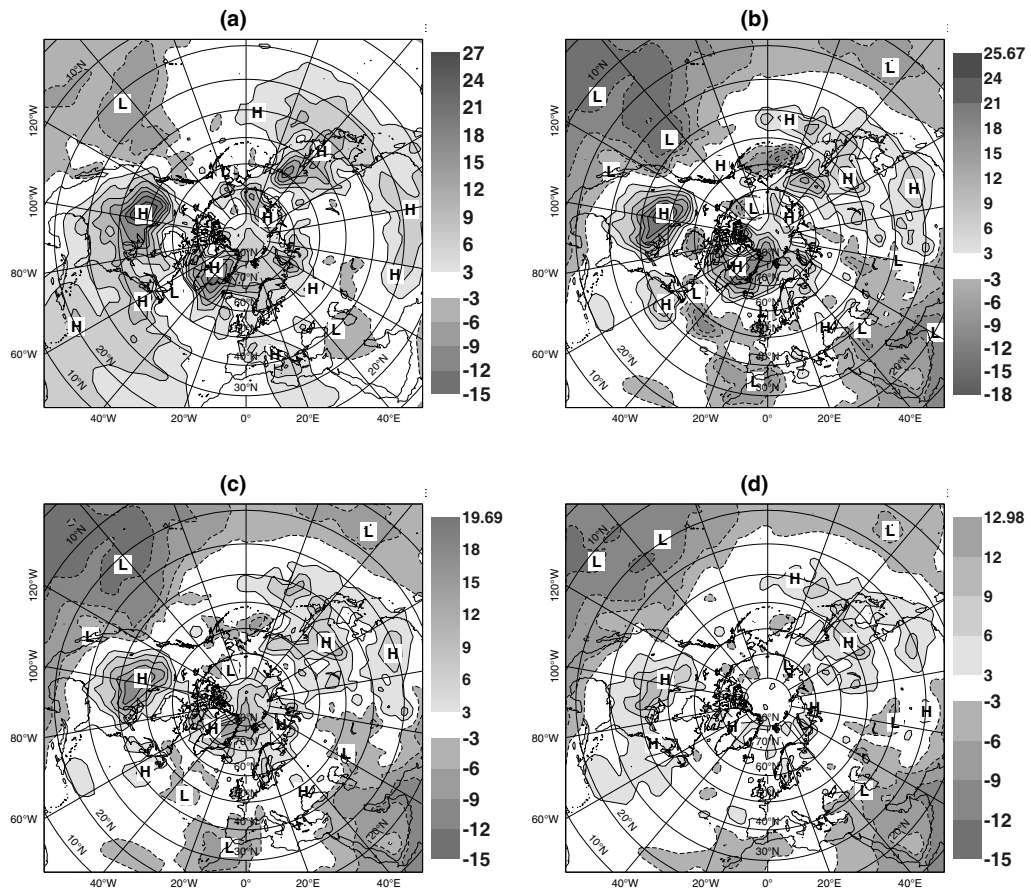


Figure 13. Systematic error (m) at 48 hours in terms of 500 hPa geopotential height during 1 May–8 June 2001 (39 cases) for (a)  $T_{L511}$  forecasts, (b) T63 forecasts, (c) initial sensitivity T63 forecasts, and (d) forcing sensitivity T63 forecasts.

substantially with maximum positive values of 25.7 m reduced to 13 m. The impact on the  $100^{\circ}\text{E}$ – $180^{\circ}\text{E}$  sector is less for both configurations. For comparison the systematic error for  $T_{L511}$  forecasts is also shown. It indicates that systematic error does not depend very much on model resolution and that even T63 computations as used above may help to understand and to reduce systematic error of models with much higher horizontal resolution.

## 5. CONCLUSIONS

In this paper a simple approach has been taken to accommodate sources of model error, such as uncertainties in the parametrization of physical processes. We assumed that during a certain forecast period the model error can be described by a time independent perturbation of the model tendencies. Note that the inclusion of an additional forcing term to the model equations is quite common in modelling to incorporate subgrid-scale dynamics in the model or to ensure a more realistic model climate (Roads 1987; Marshall and Molteni 1993).

Like initial singular vectors describe structures in the initial state that will grow rapidly (in some norm), it is also possible to define sensitive forcing perturbations. Two model integrations starting from identical initial conditions and satisfying the same model equations apart from such a forcing perturbation can produce entirely different forecasts in a few days. The constraint on forcing perturbations not to vary in time during the entire optimization time influences the structure of these optimal forcing perturbations or *forcing singular vectors* (FSVs). In fact, allowing forcings which are only active during the first time step results in identical initial and forcing singular vectors. In case the tendency perturbations are active and time independent during the entire optimization time (here 48 hours), FSVs become different from initial SVs as can be concluded by comparing unstable subspaces spanned by the leading SVs and FSVs. Also noticeable is the larger scale structure of FSVs. The typical horizontal total energy spectrum for SVs compared with the total energy norm showing a large contribution from total wave numbers around the truncation limit (T42) is absent for FSVs. Instead, FSVs and their linear response at optimization time have horizontal spectra peaking around wave number 12; there is no upscale perturbation growth as seen for SVs. In that respect the structure of FSVs is more similar to SVs which are constrained at initial time by estimates of analysis-error statistics (Barkmeijer *et al.* 1998; Palmer *et al.* 1998). However, experimentation with the Hessian norm in the sensitivity calculation (results not shown here) gave similar cost-function reduction as the regular sensitivity calculation employing the total energy norm.

The computation of FSVs may provide alternative mechanisms to explain forecast errors. Projecting forecast errors onto the subspace spanned by evolved leading SVs or FSVs showed that differences in the described part of the forecast error may occur. This became particularly noticeable when tendency perturbations were applied in the sensitivity calculation. Not only did the forced sensitivity computation result in a substantially larger reduction of the cost function which measures forecast error, the forecast also improved over areas that were not captured by the initial sensitivity. The larger cost-function reduction does, however, not imply that a constant forcing during an optimization time of 48 hours is a good approximation for model error, nor does it mean that model error plays a dominant role in producing forecast errors (Orrell *et al.* 2001). Nevertheless, one could envisage a system where initial and forced sensitivity were combined in a sequential fashion. First by searching for a suitable analysis modification and then by determining the tendency perturbation that decreases the remaining cost function. Preliminary tests in the framework of 4D-Var showed that there is scope for such an approach in that the fit to data was better when tendency perturbations were allowed, see also Derber (1989). There is also the possibility of minimizing the cost function by simultaneously allowing analysis and tendency perturbations. This, however, requires a careful balance between the analysis-error and model-error covariances.

Another area where tendency perturbations may be applied is in ensemble forecasting. Experimentation has already been performed (not shown) with the 50 member T<sub>L</sub>255L40 EPS at the ECMWF by combining analysis and tendency perturbations, the latter based on FSVs with computations starting from the operational forecast at day 3 and with an optimization period of 2 days. During the time integration of each ensemble member, a tendency perturbation comprising a mix of the leading 25 FSVs was activated from forecast day 3 onward. Averaged over 14 cases it resulted in, for example, larger ensemble spread as given by the average distance between ensemble members and ensemble mean, and improved probability scores during forecast day 3 to day 5 for geopotential height at 500 hPa.

## ACKNOWLEDGEMENTS

We are grateful to Dr Thomas Jung (ECMWF) for providing us with Fig. 13. Two anonymous reviewers are thanked for their careful reading of the manuscript and for providing us with helpful comments.

## REFERENCES

- Barkmeijer, J., Gijzen, Van M. and Bouttier, F. 1998 Singular vectors and estimates of the analysis error covariance metric. *Q. J. R. Meteorol. Soc.*, **124**, 1695–1713
- Branković, C. and Palmer, T. N. 2000 Seasonal skill and predictability of ECMWF PROVOST ensembles. *Q. J. R. Meteorol. Soc.*, **126**, 2035–2067
- Buizza, R., Petroliagis, T., Palmer, T. N., Barkmeijer, J., Hamrud, M., Hollingsworth, A., Simmons, A. and Wedi, N. 1998 Impact of model resolution and ensemble size on the performance of an ensemble prediction system. *Q. J. R. Meteorol. Soc.*, **124**, 1935–1960
- Buizza, R., Miller, M. and Palmer, T. N. 1999 Stochastic representation of model uncertainties in the ECMWF ensemble prediction system. *Q. J. R. Meteorol. Soc.*, **125**, 2887–2908
- Corti, S. and Palmer, T. N. 1997 Sensitivity analysis of atmospheric low-frequency variability. *Q. J. R. Meteorol. Soc.*, **123**, 2425–2447
- D'Andrea, F. and Vautard, R. 2000 Reducing systematic errors by empirically correcting model errors. *Tellus*, **52A**, 21–41
- DelSole, T. M. and Farrell, B. F. 1995 A stochastically excited linear system as a model for quasi-geostrophic turbulence: analytic results for one- and two-layer fluids. *J. Atmos. Sci.*, **52**, 2531–2547
- Derber, J. C. 1989 A variational continuous assimilation technique. *Mon. Weather Rev.*, **117**, 2437–2446
- Ehrendorfer, M. and Tribbia, J. J. 1997 Optimal prediction of forecast error covariances through singular vectors. *J. Atmos. Sci.*, **54**, 286–313
- Evans, R. E., Harrison, M. S. J. and Graham, R. J. 2000 Joint medium-range ensembles from the UKMO and ECMWF systems. *Mon. Weather Rev.*, **128**, 3104–3127
- Gelaro, R., Buizza, R., Palmer, T. N. and Klinker, E. 1998 Sensitivity analysis of forecast errors and the construction of optimal perturbations using singular vectors. *J. Atmos. Sci.*, **55**, 1012–1037
- Gleick, J. 1987 *Chaos*. Viking Penguin Inc., New York, USA
- Harrison, M. S. J., Palmer, T. N., Richardson, D. S. and Buizza, R. 1999 Analysis and model dependencies in medium-range ensembles: Two transplant case-studies. *Q. J. R. Meteorol. Soc.*, **125**, 2487–2515
- Hasselmann, K. 1976 Stochastic climate models. Part I. Theory. *Tellus*, **28**, 473–485
- Houtekamer, P. L., Lefaiivre, L., Derome, J., Ritchie, H. and Mitchell, H. L. 1996 A system simulation approach to ensemble prediction. *Mon. Weather Rev.*, **124**, 1225–1242
- Klinker, E. and Sardeshmukh, P. D. 1992 The diagnosis of mechanical dissipation in the atmosphere from large-scale balance requirements. *J. Atmos. Sci.*, **49**, 608–627
- Klinker, E., Rabier, F. and Gelero, R. 1998 Estimation of key analysis errors using the adjoint technique. *Q. J. R. Meteorol. Soc.*, **124**, 1909–1933
- Mahfouf, J.-F. 1999 Influence of physical processes on the tangent-linear approximation. *Tellus*, **51A**, 147–166
- Marshall, J. and Molteni, F. 1993 Toward a dynamical understanding of planetary-scale flow regimes. *J. Atmos. Sci.*, **50**, 1792–1818
- Molteni, F., Buizza, R., Palmer, T. N. and Petroliagis, T. 1996 The ECMWF ensemble prediction system: Methodology and validation. *Q. J. R. Meteorol. Soc.*, **119**, 269–298
- Moore, A. M. and Kleeman, R. 1999 Stochastic forcing of ENSO by the intraseasonal oscillation. *J. Climate*, **12**, 1199–1220
- Mylne, K. R., Evans, R. E. and Clark, R. T. 2002 Multi-model multi-analysis ensembles in quasi-operational medium-range forecasting. *Q. J. R. Meteorol. Soc.*, **128**, 361–384
- Oortwijn, J. and Barkmeijer, J. 1995 Perturbations that optimally trigger weather regimes. *J. Atmos. Sci.*, **52**, 3932–3944
- Orrell, D., Smith, L., Barkmeijer, J. and Palmer, T. 2001 Model error in weather forecasting. *Nonlinear Processes in Geophysics*, **8**, 357–371

- Palmer, T. N. 2001 A nonlinear dynamical perspective on model error: A proposal for non-local stochastic-dynamic parametrization in weather and climate prediction models. *Q. J. R. Meteorol. Soc.*, **127**, 279–304
- Palmer, T. N., Gelaro, R., Barkmeijer, J. and Buizza, R. 1998 Singular vectors, metrics and adaptive observations. *J. Atmos. Sci.*, **55**, 633–653
- Parlett, P. 1980 *The symmetric eigenvalue problem*. Series in computational mathematics. Prentice-Hall, New Jersey, USA
- Puri, K., Barkmeijer, J. and Palmer, T. N. 2001 Ensemble prediction of tropical cyclones using targeted singular vectors. *Q. J. R. Meteorol. Soc.*, **127**, 709–731
- Rabier, F., Klinker, E., Courtier, P. and Hollingsworth, A. 1996 Sensitivity of forecast errors to initial conditions. *Q. J. R. Meteorol. Soc.*, **122**, 121–150
- Richardson, D. S. 2001 Ensembles using multiple models and analyses. *Q. J. R. Meteorol. Soc.*, **127**, 1847–1864
- Roads, J. O. 1987 Predictability in the extended range. *J. Atmos. Sci.*, **44**, 1228–1251
- Simmons, A. and Hollingsworth, A. 2002 Some aspects of the improvement in skill of numerical weather prediction. *Q. J. R. Meteorol. Soc.*, **128**, 647–677
- Toth, Z. and Kalnay, E. 1997 Ensemble forecasting at NCEP and the breeding method. *Mon. Weather Rev.*, **125**, 3297–3319
- Vannitsen, S. and Toth, Z. 2002 Short-term dynamics of model errors. *J. Atmos. Sci.*, **59**, 2594–2604